**Naval Research Laboratory**
Washington, DC 20375-5320

NRL/MR/6790--07-9043

# Design of a Compact, Optically Guided, Pinched, Megawatt Class Free-Electron Laser

PHILLIP SPRANGLE
JOSEPH PEÑANO

*Beam Physics Branch*
*Plasma Physics Division*

BAHMAN HAFIZI

*Icarus Research, Inc.*
*Bethesda, Maryland*

June 8, 2007

# REPORT DOCUMENTATION PAGE

*Form Approved*
*OMB No. 0704-0188*



| 1. REPORT DATE *(DD-MM-YYYY)* | 2. REPORT TYPE | 3. DATES COVERED *(From - To)* |
|---|---|---|
| 08-06-2007 | Final | May 2004 – May 2006 |

**4. TITLE AND SUBTITLE**

Design of a Compact, Optically Guided, Pinched, Megawatt Class Free-Electron Laser

**5a. CONTRACT NUMBER**

**5b. GRANT NUMBER**

**5c. PROGRAM ELEMENT NUMBER**

**6. AUTHOR(S)**

Phillip Sprangle, Joseph Peñano, and Bahman Hafizi*

**5d. PROJECT NUMBER**
67-8915-07

**5e. TASK NUMBER**

**5f. WORK UNIT NUMBER**

**7. PERFORMING ORGANIZATION NAME(S) AND ADDRESS(ES)**

Naval Research Laboratory, Code 6790
4555 Overlook Avenue, SW
Washington, DC 20375-5320

**8. PERFORMING ORGANIZATION REPORT NUMBER**

NRL/MR/6790--07-9043

**9. SPONSORING / MONITORING AGENCY NAME(S) AND ADDRESS(ES)**

Office of Naval Research
One Liberty Center
875 North Randolph St.
Arlington, VA 22203-1995

**10. SPONSOR / MONITOR'S ACRONYM(S)**

ONR

**11. SPONSOR / MONITOR'S REPORT NUMBER(S)**

**12. DISTRIBUTION / AVAILABILITY STATEMENT**

Approved for public release; distribution is unlimited.

**13. SUPPLEMENTARY NOTES**

*Icarus Research, Inc., P.O. Box 30780, Bethesda, MD 20874-0780

**14. ABSTRACT**

A conceptual design for a compact megawatt class FEL operating within atmospheric transmission windows is presented. The proposed FEL consists of an optically guided, pinched amplifier configuration driven by an RF linac. The gain length, efficiency, electron pulse slippage and the distance between the wiggler and first relay mirror are determined for a megawatt class design. Of particular concern in the design is the overall length of the optical system, i.e., wiggler length and distance to the first relay mirror. In the present design the wiggler length is ~2 meters and the distance between the first relay mirror and the wiggler is determined by the average intensity damage threshold on the mirror. By focusing the electron beam, the optical beam can be pinched upon exiting the wiggler. The pinched optical beam has a reduced Rayleigh length which permits the first relay mirror to be relatively close to the wiggler. By pinching the optical beam and employing grazing incidence the first relay mirror can be located with ~3 meters of the wiggler. It is shown that frequency detuning can more than double the FEL efficiency. In addition, electron pulse slippage is shown to be substantially reduced in a high-gain amplifier.

**15. SUBJECT TERMS**

| | | |
|---|---|---|
| Megawatt FEL | High-gain | Pinched |
| Optically guided | Compact | Amplifier |

| 16. SECURITY CLASSIFICATION OF: | | | 17. LIMITATION OF ABSTRACT | 18. NUMBER OF PAGES | 19a. NAME OF RESPONSIBLE PERSON |
|---|---|---|---|---|---|
| a. REPORT | b. ABSTRACT | c. THIS PAGE | UL | 30 | Phillip Sprangle |
| Unclassified | Unclassified | Unclassified | | | 19b. TELEPHONE NUMBER *(include area code)* (202) 767-3493 |

**Final Technical Report**

# Design of a Compact, Optically-Guided, Pinched, Megawatt-Class Free-Electron Laser

**Prepared for**
**HIGH-ENERGY LASER JOINT TECHNOLOGY OFFICE**

**For the period**

**May 2004 to May 2006**

**Prepared by**

**Phillip Sprangle (Principal Investigator)**

**Joseph Peñano**

**Bahman Hafizi***

* Icarus Research, Inc., P.O. Box 30780, Bethesda, MD 20824-0780

Manuscript approved May 14, 2007

## CONTENTS

## SUMMARY

A conceptual design for a compact megawatt class FEL operating within atmospheric transmission windows is presented. The proposed FEL consists of an optically guided, pinched amplifier configuration driven by an RF linac. The gain length, efficiency, electron pulse slippage and the distance between the wiggler and first relay mirror are determined for a megawatt class design. Of particular concern in the design is the overall length of the optical system, i.e., wiggler length and distance to the first relay mirror. In the present design the wiggler length is ~ 2 meters and the distance between the first relay mirror and the wiggler is determined by the average intensity damage threshold on the mirror. By focusing the electron beam, the optical beam can be pinched upon exiting the wiggler. The pinched optical beam has a reduced Rayleigh length which permits the first relay mirror to be relatively close to the wiggler. By pinching the optical beam and employing grazing incidence the first relay mirror can be located within ~ 3 meters of the wiggler. It is shown that frequency detuning can more than double the FEL efficiency. In addition, electron pulse slippage is shown to be substantially reduced in a high gain amplifier.

## I. Introduction

The free electron laser (FEL) is capable of producing high average power at high efficiency without the conventional thermal management and waste issues associated with other laser systems [1]. In addition, the operating wavelength can be chosen for optimized propagation in a maritime environment [2]. These unique features make the FEL a leading candidate for naval directed energy applications [3-6].

Propagation of high power laser beams in the atmosphere involves a complex, linear and nonlinear interaction between various physical processes. The theoretical/numerical model used in this study includes the effects of aerosol and molecular scattering, aerosol heating and vaporization, thermal blooming due to aerosol and molecular absorption, atmospheric turbulence, and beam quality. These processes are modeled in a fully three-dimensional and time-dependent manner. It is found that aerosols, which consist of water, sea salt, organic matter, dust, soot, biomass smoke, urban pollutants, etc., are particularly important because they result in laser scattering, absorption and enhanced thermal blooming.

In this report we present parameters for a conceptual design of a compact, megawatt-class, optically guided, free-electron laser amplifier. There are a number important characteristics and advantages of the proposed configuration. In an optically guided FEL amplifier the filling factor, i.e., the ratio of the electron beam to the optical beam cross-sectional area, remains relatively constant throughout the wiggler region, and the radiation amplitude increases exponentially until saturation. The optical beam upon exiting the wiggler can be pinched by focusing the electron beam with external focusing fields. The Rayleigh range of the pinched optical beam can be short. As a result the first relay mirror can be placed close to the wiggler without exceeding the intensity damage threshold. The first relay mirror is a grazing incidence reflector. The FEL efficiency can be increased by tapering the wiggler. Alternatively, in a uniform wiggler, enhanced efficiency can be obtained by frequency detuning the input signal. For the power levels of interest we consider FEL operation at wavelengths 1 $\mu$m and 2.141 $\mu$m, i.e., two transmission windows associated with atmospheric water vapor. Because of propagation

and generation advantages as well as for eye safety reasons, operation at 2.141 μm may be more advantageous [4].

Recently a high-gain FEL amplifier operating in the optically guided regime has been experimentally demonstrated at the Brookhaven National Laboratory [8]. Our analysis of this experiment is in close agreement with the experimental results and will be discussed in more detail in Sec. IV.

## II. Laser Propagation in a Maritime Environment

The optimum wavelength for efficient HEL propagation depends on the atmospheric conditions and a number of inter-related physical processes which include: thermal blooming due to aerosol and molecular absorption [9], turbulence [10], aerosol and molecular scattering [11], thermal scattering due to heated aerosols, and aerosol heating and vaporization [12-15]. The relative importance of these processes depends on the parameters of the atmospheric environment which can vary significantly depending on location and time.

Atmospheric environments contain various types and concentrations of aerosols. Aerosols can absorb laser energy and conductively heat the surrounding air, resulting in an increase in thermal blooming of the HEL beam [2,16]. In general, aerosols consist of hygroscopic and non-hygroscopic particles of various sizes and chemical compositions. Oceanic aerosols consist of sea salt, water, and organic material. Non-hygroscopic aerosols are composed of dust, soot, biomass smoke, and other carbon-based compounds. These aerosols typically have much larger absorption coefficients than water-based aerosols. While they are normally present in continental, rural and urban environments, dust aerosols can also be present in maritime environments hundreds of miles from shore [17].

### i) Maritime Atmosphere Model

The Advanced Navy Aerosol Model (ANAM) is used to model the near-surface maritime environment [18]. The ANAM aerosol distribution is comprised of various modes which represent aerosols of different compositions and sizes. These aerosol modes will absorb laser energy and vaporize at different rates. The aerosol size

distribution function, $F(R,t) = \sum_{j=0}^{4} F_j(R,t)$, where $R$ is the aerosol radius, is represented as a superposition of five "modes" with each mode representing aerosols with a particular physical composition and origin. The aerosol distribution can evolve with time, due to vaporization for example, the aerosol absorption and scattering coefficients are also time-dependent. Mode 0 represents dust particles of continental origin, mode 1 represents water-soluble aerosols, and modes 2-4 represent marine aerosols (sea salt and water) that result from different processes.

We use MODTRAN to calculate the molecular absorption and scattering coefficients [19]. Figure 1 plots the gross scattering and absorption coefficients due to aerosol and molecular contributions in the water vapor transmission windows, $\lambda = 1.045, 1.625$ and $2.141\mu m$. The gross scattering and absorption coefficients that we obtain are comparable with *in situ* measurements [20, 21].

**ii) HEL Propagation Simulations**

To simulate HEL propagation we use the **H**igh **E**nergy **L**aser **C**ode for **A**tmospheric **P**ropagation, HELCAP [2,22], developed at the Naval Research Laboratory. HELCAP includes the effects of i) aerosol and molecular scattering, ii) aerosol heating and vaporization, iii) thermal blooming due to both aerosol and molecular absorption, iv) atmospheric turbulence, and v) laser beam quality, i.e., all of the effects discussed in the preceeding section. It is the first HEL propagation model which integrates all these physical processes in a fully three-dimensional, time-dependent manner. In modeling the aerosol effects, we account for the aerosol distribution and the various aerosol modes (water-based, dust, soot, etc.).

In HELCAP the laser electric field is represented as $\mathbf{E} = A(x,y,z,t)\exp[\, i(\omega z/c - \omega t)]\, \hat{\mathbf{e}}_x/2 + c.c.$, where $\omega = 2\pi c/\lambda$ is the laser frequency, $\hat{\mathbf{e}}_x$ is a unit polarization vector in the $x$ direction, $A(x,y,z,t)$ is the complex laser amplitude and the laser intensity is $I = c\,A\,A^*/8\pi$. HELCAP solves a nonlinear Schrödinger-like equation which has the form

$$\frac{\partial A}{\partial z} = \frac{ic}{2\omega}\nabla_{\perp}^{2}A + \left[ i\frac{\omega}{c}(\delta n_T + \delta n_{TB}) - \frac{1}{2}(\alpha + \beta) \right] A,$$

where $\alpha = \alpha_m + \alpha_A$ is the total absorption coefficient, $\beta = \beta_m + \beta_A$ is the total scattering coefficient, and $\delta n_T$ and $\delta n_{TB}$ denote the refractive index variation due to atmospheric turbulence and thermal blooming respectively. $\alpha_m$ ($\alpha_A$) is the molecular (aerosol) absorption coefficient. $\beta_m$ ($\beta_A$) is the molecular (aerosol) scattering coefficient. The quantities $\delta n_T$, $\delta n_{TB}$, $\alpha$, and $\beta$ are space and time-dependent and determined self-consistently in the presence of aerosol heating and vaporization.

The transmitted power at the source is denoted by $P$ and the laser is focused onto a remote target at a range of 5 km (see Fig. 2). The target is taken to be circular with an area of 100 cm$^2$. The propagation direction is along the z-axis and a uniform transverse wind, with velocity $V_W$ = 5 m/sec is directed along the y-axis. Atmospheric turbulence is modeled by a Kolmogorov spectrum with structure constant $C_n^2 = 10^{-15}$ m$^{-2/3}$. The pointing jitter associated with the laser beam is taken to have an angular spread of 2 μrad and a white noise temporal spectrum.

Figure 3 plots the average power on target versus the transmitted power, $P$, for the three wavelengths of interest. Our results show that for a maritime environment, the optimum wavelength depends on the transmitted power. For $P$ < 1.5 MW, propagation is mostly affected by aerosol scattering and the average power on target increases with $P$. In this regime, the 1.625 μm, and 2.141 μm wavelengths provide slightly greater power on target than 1.045 μm. This is due to the lower aerosol scattering coefficient associated with the longer wavelengths. For $P$ < 1.5 MW, the propagation efficiency is roughly 50% for the three wavelengths considered. For example, $P$ = 1 MW results in $\langle P_{\text{target}} \rangle \sim 0.55$ MW for $\lambda = 1.625\,\mu\text{m}$ and $\lambda = 2.141\,\mu\text{m}$. However, for $P$ > 1.5 MW, thermal blooming becomes important. In this high power regime the optimum wavelength is 1.045 μm due to the lower molecular absorption coefficient in that water vapor window. For $P$ = 3 MW, $\langle P_{\text{target}} \rangle \sim 1$ MW for 1.045 μm while $\langle P_{\text{target}} \rangle \sim 0.8$ MW for 1.625 μm and 2.141 μm.

For the power levels of interest, $P \leq 1.5\,\mathrm{MW}$ average power, it may be advantageous to operate the FEL at $2.141\,\mu\mathrm{m}$. For maritime propagation there is no distinct advantage in operating the FEL at either $1.045\,\mu\mathrm{m}$ or $1.625\,\mu\mathrm{m}$. However, for $P \geq 1.5\,\mathrm{MW}$, operating at $1\,\mu\mathrm{m}$ leads to greater propagation efficiency.

## III. Optically Guided FEL Amplifier

Using the Source Dependent Expansion (SDE) formulation [23], expressions for the optical growth rate, wavenumber shift, spot size and optical curvature of the optical beam in an FEL amplifier are obtained in the Appendix. These results are used to design a compact MW FEL in the optically guided, high gain regime, i.e., having a matched optical spot size. In addition, focusing the electron beam at the wiggler exit is shown to result in a pinched optical beam with a shortened Rayleigh range. A schematic diagram of the FEL amplifier configuration is shown in Fig. 4. Finally, it is shown that by frequency detuning the FEL efficiency can be more than doubled. The following discussion motivates the design parameters listed in Tables I – V. For illustrative purposes, the numbers given in the text correspond to a resonant wavelength of $\lambda = 2.141\ \mu m$ with $\Delta\omega = 0$ unless otherwise stated.

### i) Operating Wavelength

In the present design the resonant operating wavelength of a linearly polarized optical beam is $\lambda = \lambda_w(1+K^2/2)/2\gamma^2$, where $\gamma = E_b[\mathrm{MeV}]/0.511 + 1$ is the total relativistic mass factor. Design parameters for $\lambda = 1\ \mu m$ and $\lambda = 2.141\ \mu m$ are listed in Tables I-V.

### ii) Gain Length

The power gain length in the optically guided regime, in the absence of frequency detuning $(\Delta\omega = 0)$, is

$$L_e = 1/2\Gamma = \frac{\lambda_w}{8\pi}\left(\frac{(2+3f)}{2(1+2f)^2}\left(\frac{\nu}{\gamma}\right)^{1/2}\frac{K}{\sqrt{1+K^2/2}}\right)^{-1} = 14\,\mathrm{cm}, \qquad (1)$$

where $f = R_b^2 / R_L^2 \leq 1$ is the filling factor, $\nu = I_b[\mathrm{kA}]/17$ is Budker's parameter, $I_b$ is the electron beam current in kA, $K = q B_W \lambda_w / 2\pi mc^2 = 1.9$ is the wiggler strength parameter, $B_W = 5\,\mathrm{kG}$ is the wiggler field and $\lambda_w = 4\,\mathrm{cm}$ is the wiggler period. The transverse profiles of the optical and electron beam are Gaussian with radii $R_L$ and $R_b$, respectively [see Eqs. (A2) and (A4)].

**iii) FEL Efficiency**

In the optically guided, high gain regime the efficiency of conversion from electron beam power to optical power is given by [3,24]

$$\eta = \frac{\lambda_w \Delta k}{2\pi} = \frac{f^{1/2}(2+3f)^{1/2}}{(1+2f)^2}\left(\frac{\nu}{\gamma}\right)^{1/2} \frac{K}{\sqrt{1+K^2/2}} = 0.8\%. \qquad (2)$$

Here, $\Delta k$ is the wavenumber shift, defined in Eq. (A3). Free-electron laser efficiency can be increased by tapering the wiggler [5, 24, 25] or by frequency detuning [3,24].

**iv) Optical Guiding**

The FEL optical beam can undergo refractive guiding within the wiggler. An envelope equation for the optical beam spot size can be obtained by using the results in the Appendix, and the condition for a matched optical beam can be obtained. For optical guiding the power gain length is nearly equal to the free space Rayleigh range, that is

$$L_e = \frac{(2+3f)^{1/2}}{2f^{1/2}(1+2f)} Z_R, \qquad (3)$$

where $Z_R = \pi R_L^2 / \lambda = 22\,\mathrm{cm}$ is the Rayleigh range. The optical guiding condition in Eq. (3) can be rewritten in terms of the beam current,

$$I_b[kA] = 1.1\times10^{-2} \frac{f^3(1+2f)^6}{(2+3f)^3}\left(\frac{\lambda_w}{R_b}\right)^4 \frac{\left(1+K^2/2\right)^3}{\gamma^3 K^2} = 1\,\mathrm{kA}. \qquad (4)$$

In addition, the centroid of the FEL optical beam can be steered by gradually bending the electron beam.

**v) Saturated Peak and Average Optical Power**

The peak optical power at saturation is $P = \eta I_b V_b = 1\text{GW}$, where $V_b = 81\text{MV}$ is the electron beam voltage. The average power at saturation is

$$\langle P \rangle = \eta D I_b V_b = 1.5\text{MW}, \tag{5}$$

where $D = 1.5\times10^{-3}$ is the duty factor and $\eta = 1.2\%$ ($\Delta\omega/\omega = -1.5\%$).

**vi) Electron Pulse Slippage (Lethargy)**

In the high-gain regime electron slippage (lethargy) is shown to be significantly less than in the low gain regime and is not a concern for this design. The slippage length, i.e., the separation between the optical and electron pulse, is $S \equiv (\mathrm{v}_g - \mathrm{v}_z) L_w / c$, where $\mathrm{v}_g = \partial\omega/\partial k$ is the optical pulse group velocity, $\mathrm{v}_z \cong c(1 - 1/2\gamma_z^2)$ is the axial electron beam velocity, and $\gamma_z = \gamma/\sqrt{1 + (K^2/2)}$. Making use of the high gain FEL dispersion relation [3,24], the group velocity is $\mathrm{v}_g \cong c\left(1 - 1/3\gamma_z^2 - (\lambda/\pi R_L)^2/2\right)$, and the slippage length is

$$S = \lambda N_w \left( \frac{1}{3} - \left( \frac{\lambda \gamma_z}{\pi R_L} \right)^2 \right) \leq 27\mu m, \tag{6}$$

where $N_w = L_w/\lambda_w$ is the number of wiggler periods. The well known slippage length in the low gain regime is $\lambda N_w$. Slippage in the high gain regime is reduced by more than a factor of three.

**vii) Pinched Optical Beam**

The intensity on the first relay mirror must be below a damage threshold level. To further reduce the intensity on the mirror the optical beam can be pinched at the wiggler exit in order to shorten the Rayleigh range [3-5]. By employing external focusing fields near the wiggler exit the electron beam and in turn the optical beam can be pinched. Making use of grazing incidence geometry the intensity on the mirror can be further reduced.

The spot size of the optical beam $R_L(z)$ [obtained by solving Eqs. (A5), (A6) and (A8)] and the radius of the electron beam $R_b(z)$ are plotted as functions of the propagation distance $z$ in Fig. 5. The entrance to the wiggler is at $z = 0$ and extends to $z = L_w = 1.5\,\mathrm{m}$. In Fig. 5(a) the radius of the electron beam is constant and the optical beam is guided through the wiggler with a constant spot size. Upon exiting the wiggler, the optical beam diffracts. In the example of Fig. 5(b) the electron beam is focused by external fields applied near the wiggler exit. This pinches the optical beam and as a result, the optical beam diffracts more rapidly than in the unpinched example.

**viii) Optical Beam Quality and Beam Spreading**

It is common practice to characterize the higher order modal content of a laser beam by a beam quality parameter denoted by $M^2$. The quantity $M^2 \geq 1$ is a "times diffraction-limited" parameter which, for a fundamental Gaussian beam, is unity. Upon exiting the FEL interaction region, i.e., wiggler, the spatial spreading of the optical beam is given by

$$W^2(z) \equiv \frac{2}{P}\int_0^\infty r^2\, I(r,z)\, 2\pi r\, dr = W_o^2 + M^4\,\theta_D^2\,(z - L_w)^2, \qquad (7)$$

where $W$ is the laser beam spot size, $P$ is the power and $I$ is the intensity. In Eq.( 7), $W_o$ is the minimum spot size at $z = L_w$, $\theta_D = \lambda/(\pi W_o)$ is the diffraction (spreading) angle of an ideal Gaussian beam and $M^2$ is a measure of the beam quality. For a non-ideal optical beam the diffraction angle is $M^2\,\theta_D$ at the exit of the wiggler. Using the paraxial wave equation in Sec. II, it can be shown that the general expression for the evolution of $M^2$ is

$$M^2(z) = \left\{ \frac{4\pi^2}{P^2}\left[ \left( \int_0^\infty I r^3\, dr \right) \int_0^\infty \left( \left( \frac{\partial I^{1/2}}{\partial r} \right)^2 + \left( \frac{\partial \phi}{\partial r} \right)^2 I \right) r\, dr - \left( \int_0^\infty I \frac{\partial \phi}{\partial r} r^2\, dr \right)^2 \right] \right\}^{1/2}, \qquad (8)$$

where the complex laser amplitude has been expressed in terms of the intensity, $I$, and phase, $\phi$, as $A \sim I^{1/2}(r,z)\exp(i\phi(r,z))$. When the laser beam propagates in a region of uniform refractive index, i.e., outside of the wiggler, $M^2$ is constant. Simulations using the FEL code MEDUSA indicate that the beam quality of an optically guided FEL beam is fairly good. For parameters similar to those in Table I and II , simulation results indicate the $M^2 \approx 1.5$ at the exit of the wiggler [26]

**ix) Distance Between First Relay Mirror and Wiggler**

To avoid damage, the distance between the wiggler and relay mirror must exceed

$$L_{\text{relay}} = \frac{Z_R}{M^2}\left(\frac{\langle I\rangle}{\langle I_{\text{damage}}\rangle}\right)^{1/2} \sin^{1/2}\Theta \ , \tag{9}$$

where $\Theta$ is the tilt angle (Fig. 4), $Z_R = \pi R_L^2/\lambda$ is the Rayleigh range at the exit of the wiggler, $\langle I\rangle = 2\langle P\rangle/\pi R_L^2$ is the average intensity at exit of the wiggler, and $\langle I_{\text{damage}}\rangle = 50\ \text{kW/cm}^2$ is the average intensity damage threshold of the mirror. Using the parameters in Tables I, II, and III, we obtain (see Table IV) for an unpinched optical beam,

$$L_{relay} = \begin{cases} 15\,\text{m}, & \Theta = 45^\circ \\ 8\,\text{m}, & \Theta = 5^\circ \end{cases} , \tag{10}$$

and for a pinched beam

$$L_{relay} = \begin{cases} 5\,\text{m}, & \Theta = 45^\circ \\ 3\,\text{m}, & \Theta = 5^\circ \end{cases} . \tag{11}$$

For operation at $\lambda = 1\ \mu m$ ,

$$L_{relay} = \begin{cases} 27\,\text{m}, & \Theta = 45^\circ \\ 10\,\text{m}, & \Theta = 5^\circ \end{cases} , \tag{12}$$

and for an unpinched beam, and

$$L_{relay} = \begin{cases} 11\,\text{m}, & \Theta = 45^\circ \\ 4\,\text{m}, & \Theta = 5^\circ \end{cases} \tag{13}$$

for a pinched beam (see Table V).

**x) Frequency Detuning and Efficiency Enhancement**

In an FEL the efficiency can be increased by operating at a frequency that is detuned from the resonant value $\omega_R = 2\pi c/\lambda$. In general, however, operating off-resonance leads to a reduction in the growth rate [1]. If the operating frequency is denoted by $\omega$, the modification to the present analysis is the replacement of the wavenumber shift $\Delta k$ with $\Delta k - (\omega - \omega_R)/(2c\gamma_z^2)$ in the expression for the efficiency in Eq. (2) and in Eq. (A7) which leads to the dispersion relation. Note that the left hand side of Eq. (A8) is not changed.

To demonstrate these effects, Fig. 6 shows (a) the efficiency, (b) the gain length and (c) the filling factor as functions of the relative frequency shift $(\omega - \omega_R)/\omega_R$ for $\lambda = 1\ \mu\text{m}$. The minimum gain length is obtained near the resonance frequency, as indicated in Fig. 6(b). The efficiency, on the other hand, is observed to rise monotonically as the frequency is reduced relative to the resonant value. There is also a reduction in the filling factor for increasingly-negative frequency shifts. That is, operating at lower frequencies reduces the guiding effect and thus leads to an increase in the optical spot size.

## IV. Discussion and Conclusions

Conceptual design parameters for a compact MW-class FEL amplifier operating in the optically guided, high gain regime are presented. The design presented here assumes that the FEL amplifier is driven by a high quality RF linac generated electron beam. Optical guiding allows the interaction length to be sufficiently long to achieve substantial growth of the input signal. Electron pulse slippage, which can limit the FEL interaction length, is shown to be significantly reduced for a high gain amplifier. By pinching the optical beam at the wiggler exit the Rayleigh range is shortened, thus reducing the required distance to the first relay mirror. The optical beam can be pinched

by focusing the electron beam with external magnetic fields or by utilizing the betatron oscillation of the electron beam envelope. Grazing incidence geometry permits a further reduction in intensity to avoid damage to the mirror.

We find that operation at 2.141 μm is advantageous because of propagation and generation considerations as well as for eye safety reasons. For a 1 kA, 81 MV electron beam, a wiggler field of 5 kG, and a frequency detuning of $-1.5\%$, the power gain length is 14 cm, the intrinsic efficiency is ~ 1.2%, the optical output power is 1 GW, and the average output power is 1.5 MW, assuming a duty factor of $1.5\times10^{-3}$ for the RF linac. Focusing the electron beam radius down by a factor ~ 3 at the exit of the ~ 1.5 m wiggler reduces the optical beam Rayleigh range by a factor of ~ 4. Depending on the mirror grazing angle and the optical beam quality, the distance from the wiggler exit to the first relay mirror can be < 3 m. The length of the optical system, which includes the amplifier section and the first relay mirror, can be < 5 m.

A recent experiment at the Brookhaven National Laboratory (BNL) has demonstrated the optically guided, high-gain FEL amplifier concept. This experiment utilized a 10 m long wiggler and an S-band RF linac that produced a 100 MeV, 300A electron pulse of radius 0.2 mm. The wiggler period and strength parameter were 3.9 cm and 1.1, respectively. Experiments showed optical guiding in a high gain FEL amplifier operating at $\lambda = 0.8\,\mu m$ using a Ti-Sapphire laser as the seed. Dipole steering magnets located along the wiggler were used to deflect the electron beam by ~ 1mrad and the light beam was shown to be steered and guided by the electron beam. The transverse profile of the optically guided light beam was shown to be less than half the size of an unguided diffracting light beam. The power peak output power was ~150 MW [8]. Our simulations of the BNL experiment predict a power e-folding length of 42 cm, a guided spot size of 0.24 mm (1/e of intensity), and a peak power output of ~180 MW, in close agreement with the experimental results.

Simulations of the FEL amplifier, taking into account emittance, energy spread, and non-uniformity of the optical guiding due to variation of the electron current within the pulse, are required to fully evaluate the present design. Also, while estimates indicate that a modest external magnetic field is sufficient to focus the beam, more refined

analysis is required to design the pinch region of the wiggler. In the absence of optical pinching, the distance to the first relay mirror can be < 10 m.

## Acknowledgments

This work was sponsored by the High Energy Laser Joint Technology Office and Office of Naval Research.

## Appendix

The source dependent expansion (SDE) formulation [23] can be used to analyze the dynamics of the optical beam in FELs. A summary of the principal SDE equations is given in this appendix. For a planar wiggler the electric field of the radiation can be taken to be linearly polarized, and given by

$$E(r,z) = \tfrac{1}{2} A(r,z) \exp\big(i\omega(z/c - t)\big) + c.c. \tag{A1}$$

For the fundamental Gaussian mode the complex envelope $E_o(r,z)$ is written as

$$A(r,z) = A_o \exp\big(i\Psi(z)\big) \exp\big(-(1 - i\alpha(z))r^2 / R_L^2(z)\big), \tag{A2}$$

where $A_o$ is the amplitude on axis,

$$\Psi(z) = \int_0^z \big(\Delta k(z') - i\Gamma(z')\big)dz', \tag{A3}$$

$\Delta k(z)$ is the wavenumber shift, $\Gamma(z)$ is the spatial growth rate, $\alpha(z)$ is related to the curvature of the optical wavefronts and $R_L(z)$ is the spot size of the beam. To allow for an electron beam with a radius $R_b(z)$ that varies along the propagation axis, the electron beam density is taken to be

$$n_b(z,r) = n_b(0)\big(R_b^2(0)/R_b^2(z)\big)\exp\big(-r^2/R_b^2(z)\big). \tag{A4}$$

The SDE equations for the spot size and $\alpha(z)$ are given by [3]

$$\frac{dR_L(z)}{dz} - \frac{2c\alpha(z)}{\omega}\frac{1}{R_L(z)} = -H_I(z)R_L(z), \tag{A5}$$

and

$$\frac{d\alpha(z)}{dz} - \left(\frac{2c}{\omega}\right)\frac{1+\alpha^2(z)}{R_L^2(z)} = 2\big(H_R(z) - \alpha(z)H_I(z)\big), \tag{A6}$$

respectively. Here,

$$H(z) = 4\frac{v}{\gamma}\frac{c}{\omega}\left(\frac{K^2 k_w^2}{1 + K^2/2}\right)\frac{1}{R_b^2(z)}\frac{f(z)}{\big(1 + 2f(z)\big)^2}\frac{1}{\big(\Delta k(z) - i\Gamma(z)\big)^2}, \tag{A7}$$

where $\nu = I_b[\mathrm{kA}]/17$ is Budker's parameter, $k_w = 2\pi/\lambda_w$, $f(z) = R_b^2(z)/R_L^2(z)$ is the filling factor and the subscripts R and I denote real and imaginary parts. The final SDE equation for the phase shift and growth rate is given by

$$\Delta k(z) - i\Gamma(z) + \left(\frac{c}{\omega}\right)\frac{(1+\alpha^2(z))}{R_L^2(z)} - i\frac{(1-i\alpha(z))}{R_L(z)}\frac{dR_L(z)}{dz} + \frac{1}{2}\frac{d\alpha(z)}{dz} = -(1+2f(z))H(z) \tag{A8}$$

Equations (A5), (A6) and (A8) describe the optical beam in the high gain FEL amplifier. The electron beam can be focused to produce a pinched optical beam.

## REFERENCES


[1] C.W. Roberson and P. Sprangle, "A review of free-electron lasers," Phys. Fluids B, **1**, pp. 3-42 (1989).

[2] Sprangle, P., J.R. Peñano and B. Hafizi, "Optimum Wavelength and Power for Efficient Laser Propagation in Various Atmospheric Environments," NRL Technical Memorandum NR/MR/6790-05-8907.

[3] P. Sprangle, B. Hafizi, J. Peñano, IEEE Journal of Quantum Electronics 40, 1739 (2004)

[4] P. Sprangle, J. Peñano, B. Hafizi, Journal of Directed Energy **2**, 119 (2006); P. Sprangle, J. Peñano, B. Hafizi, NRL Technical Memorandum NR/MR/6790-05-8929

[5] D.C. Nguyen and H.P. Freund, Nucl. Instrum. Methods Phys. Res. A, **507**, 120 (2003); D.C. Nguyen, S.S. Kurenroy, L.M. Young and H.P. Freund, J. Directed Energy **1**, 171 (2004).

[6] W.B. Colson, A. Todd and G.R. Neil, "A high power free electron laser using a short Rayleigh length," in *Free Electron Lasers 2001*, M. Brunken, H. Genz and A. Richter, Eds. Holland: Elsevier Science, 2002, pp. II-9-II10; J. Blau, V. Bouras, A. Kalfoutzos, G. Allgaier, T. Fontana, P.P. Crooker and W.B. Colson, Nucl. Instrum. Methods Phys. Res. A, **507**, 44 (2003).

[7] G.R. Neil, C.L. Bohn, S.V. Benson, G. Biallas, D. Douglas, H.F. Dylla, R. Evans, J. Fugitt, A. Grippo, J. Gubeli, R. Hill, K. Jordan, G.A. Krafft, R. Li, L. Merminga, P. Piot, J. Preble, M. Shinn, T. Siggins, R. Walker and B. Yunn, Phys. Rev. Lett. **84**, 662 (2000).

[8] J. Murphy, Private Communication (2005); X.J. Wang, et. al, "Megawatt Class FEL Amplifier Experiments at the NSLS SDL", presented at the Directed Energy Professional Society Symposium, Lihue, Hawaii, Nov. 2005.

[9] Smith, D.C., "High-Power Laser Propagation - Thermal Blooming," Proc. IEEE **65**, 1679 (1977)

[10] The Infrared and Electro-Optical Systems Handbook, vol. 2, edited by F.G. Smith, Environmental Research Institute of Michigan, Ann Arbor, MI, and SPIE Optical Engineering Press, Bellingham, WA (1993).

[11] Measures, R.M., "Laser Remote Sensing, Fundamentals and Applications," Krieger Publishing, Malabar, FL (1992)

[12] Williams, F. A, Int. J. Heat Mass Transfer. **8**, 575 (1965).

[13] Caledonia, G.E. and J.D. Teare, J. Heat Transfer **99**, 281 (1977).

[14] Armstrong, R.L., Appl. Optics **23**, 148 (1984); Armstrong, R.L., J. Appl. Phys. **56**, 2142 (1984); Armstrong, R.L., S.A.W. Gerstl and A. Zardecki, J. Opt. Soc. Am. A **2**, 1739 (1985).

[15] Davies, S.C. and J.R. Brock, App. Optics **26**, 786 (1987)

[16] Brown R.T. and D.C. Smith, J. App. Phys. **46**, 402 (1975)

[17] Reid, J.S., D.L. Westphal, R.M. Paulus, S. Tsay and A. van Eijk, "Preliminary Evaluation of the Impacts of Aerosol Particles on Laser Performance in the Coastal Marine Boundary Layer," Naval Research Laboratory, Monterey, CA 93943-5502, NRL/MR/7534—04-8803, Jun. 2004.

[18] van Eijk, A.M.J. and L.H. Cohen, "The ANAM-3.0 Development," TNO Physics and Electronics Laboratory, Jun. 2005; Piazzola, J., M.J. van Eijk, G. de Leeuw, Opt. Eng. **39**, 1620 (2000).

[19] Berk, A., G.P. Anderson, P.K. Acharya, J.H. Chetwynd, L.S. Bernstein, E.P. Shettle, M.W. Matthew, and S.M. Adler-Golden, "MODTRAN4 User's Manual," Air Force Research Laboratory, Hanscom AFB, MA (2000)

[20] Doss-Hammel, S., D. Tsintikidis, D. Merritt and J. Fontana, "Atmospheric Characterization for High Energy Laser Beam Propagation in the maritime Environment," Proc. SPIE, vol. 5552, SPIE, Bellingham, WA, 2004, p. 208.

[21] Bodhaine, B.A., J. Geophys. Res. **100**, 8967 (1995); Quinn, P.K., D. J. Coffman, T. S. Bates, E. J. Welton, D. S. Covert, T. L. Miller, J. E. Johnson, S. Maria, L. Russell, R. Arimoto, C. M. Carrico, M. J. Rood, J. Anderson, J. Geophys. Res. 109, D19S01 (2004)

[22] Sprangle, P., J. R. Peñano, A. Ting, B. Hafizi and D.F. Gordon, Journal of Directed Energy 1, **73** (2003); P. Sprangle, J.R. Peñano and B. Hafizi, Phys. Rev. E, **66**,

046418 (2002); Peñano, J.R., P. Sprangle, B. Hafizi, A. Ting, D.F. Gordon and C.A. Kapetanakos, Phys. Plasmas **11,** 2865 (2004); P. Sprangle, J.R. Peñano, A. Ting, B. Hafizi and D.F. Gordon, J. Directed Energy, **1**, 73 (2003).

[23] Sprangle, P., A. Ting and C.M. Tang, Phys. Rev. Lett., **59**, 202 (1987).

[24] Sprangle, P., C.M. Tang and W.M. Manheimer, Phys. Rev. A **21**, 302 (1980); P. Sprangle, C.M. Tang and C.W. Roberson, Nucl. Instrum. Methods Phys. Res. A **239**, 1 (1985).

[25] Orzechowski, T.J., B.R. Anderson, J.C. Clark, W.M. Fawley, A.C. Paul, D. Prosnitz, E.T. Scharlemann, S.M. Yarema, D.B. Hopkins, A.M. Sessler and J.S. Wurtele, Phys. Rev. Lett. **57**, 2172 (1986).

[26] Sprangle, P., "A Compact Optically Guided Pinched Megawatt Class FEL," Eighth Annual Directed Energy Symposium, Lihue, Hawaii, November 14-18, 2005

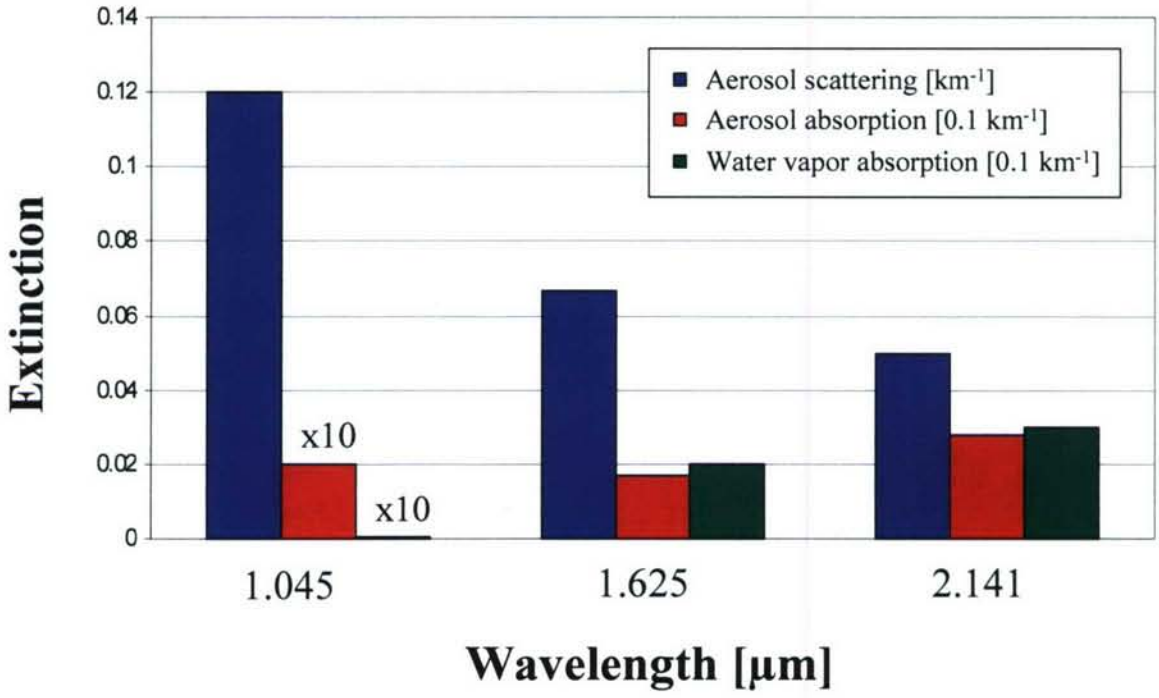


Figure 1: Aerosol scattering, aerosol absorption, and water vapor (molecular) absorption coefficients used for the model maritime environment of the propagation simulation. Aerosol scattering and absorption are calculated using ANAM, water vapor absorption is calculated using MODTRAN4.

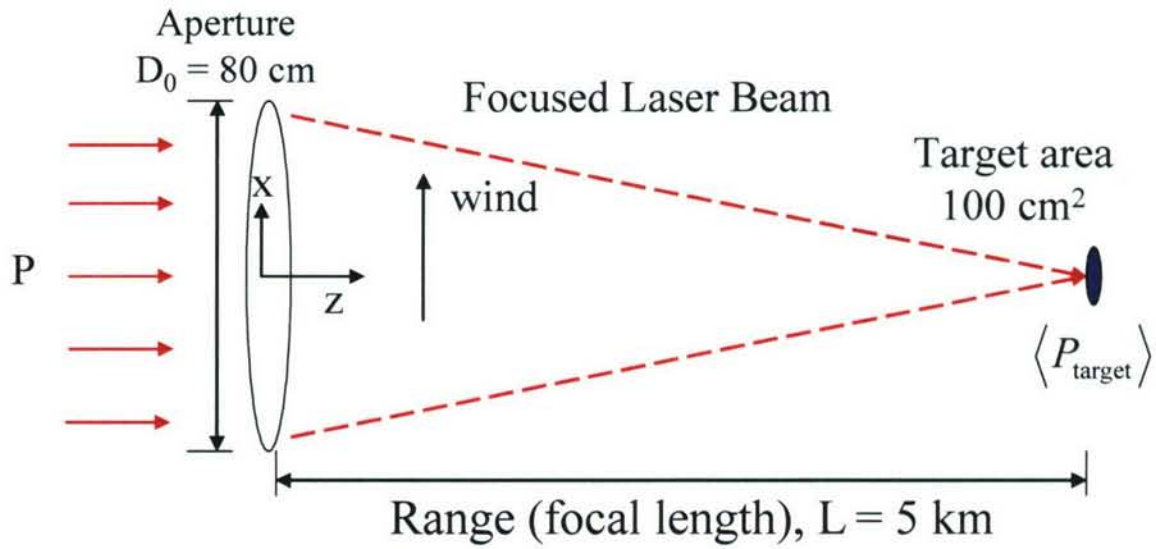


Figure 2: Schematic of laser and target configuration used in the full scale propagation simulations.

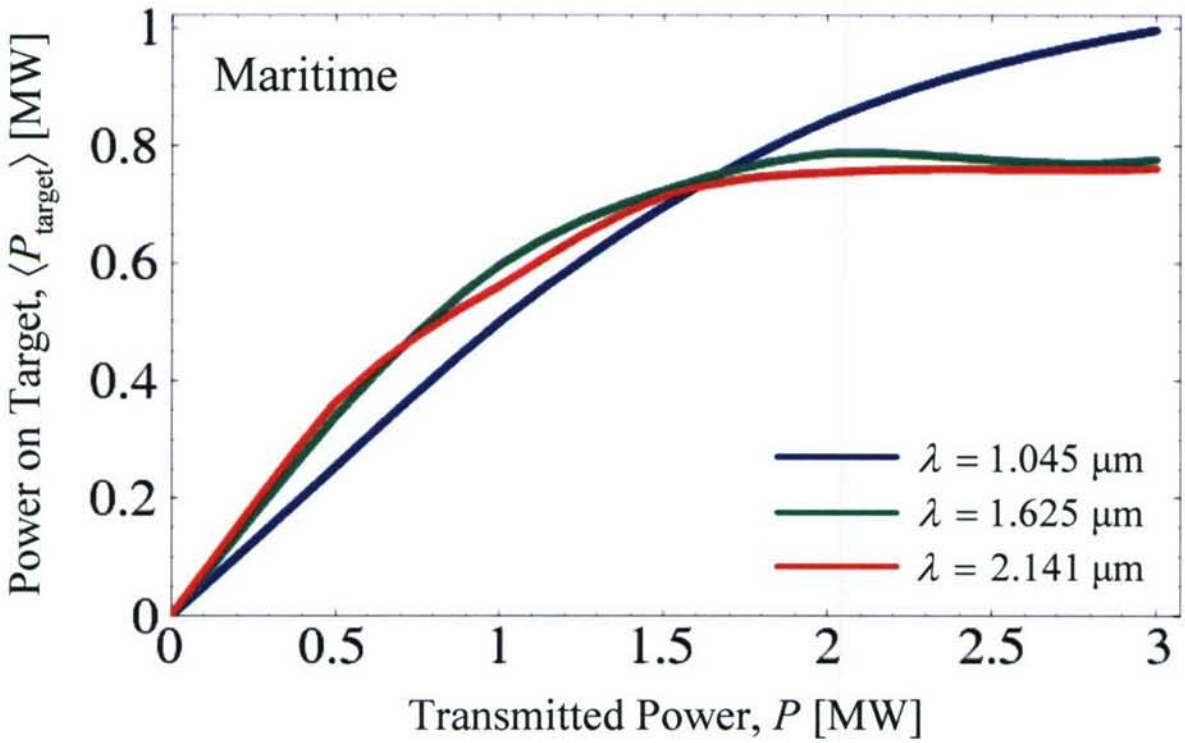


Figure 3: Average power on target, $\langle P_{\text{target}} \rangle$, versus transmitted power, $P$, in a maritime environment for the wavelengths $\lambda$ = 1.045, 1.625, 2.141 μm. Initial beam profile has $R_0$ = 50 cm, $D_0$ = 80 cm. Simulation geometry is shown in Fig. 2. Target range, L = 5 km; beam focus = 5 km; target area = 100 cm$^2$; wind speed, $V_W$ = 5 m/sec; turbulence strength, $C_n^2 = 10^{-15}$ m$^{-2/3}$; pointing jitter angular amplitude = 2 μrad (white noise).

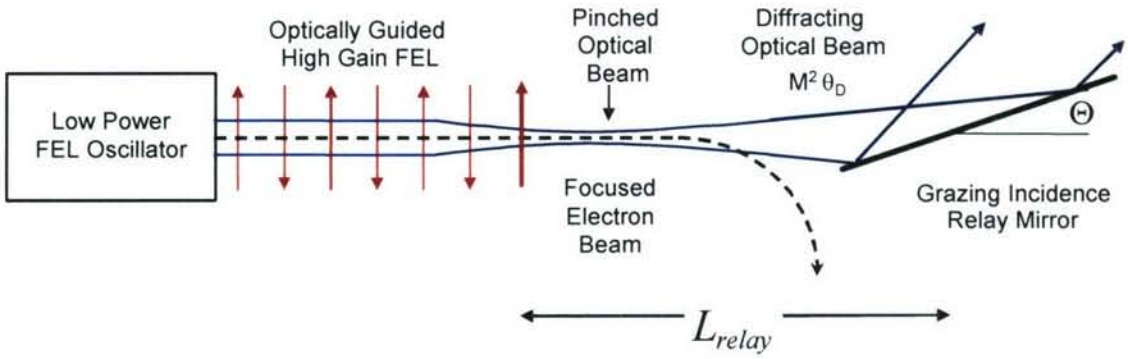


Figure 4. Schematic of high gain FEL amplifier with a grazing relay mirror. The input signal can be obtained a low average power FEL oscillator. The radiation beam is optically guided in the wiggler and optically pinched at the exit. The pinched optical beam has a shortened Rayleigh range and undergoes rapid diffraction upon exiting the wiggler. Employing a grazing incidence configuration the resultant footprint on the relay mirror can be made sufficiently large to avoid damage.

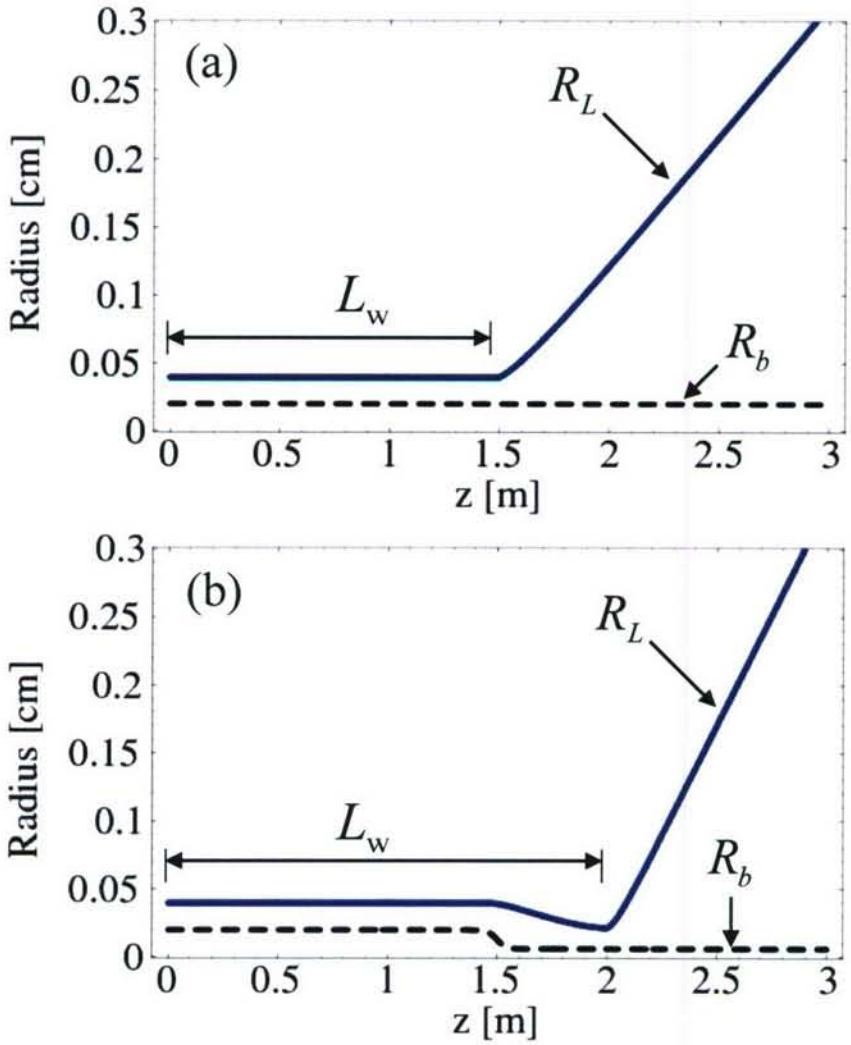


Figure 5. Plots of optical beam radius ( $R_L$ ) and electron beam radius ( $R_b$ ) versus propagation distance $z$. Wiggler entrance is at $z = 0$ and the exit is at $z = L_w \sim 1.5\,\mathrm{m}$. The FEL operates in the high-gain regime, where the optical beam maintains a constant spot size by optical guiding. Outside the wiggler the optical beam diffracts and spreads transversely, as indicated in (a). By focusing the electron beam at the wiggler exit the optical beam can be pinched down to $R_{\mathrm{L,pinch}} = 0.21\,\mathrm{mm}$ as indicated in (b). The pinched optical beam diffracts more rapidly compared to the unpinched example, i.e., has a shorter Rayleigh range, $Z_{\mathrm{R,pinch}} = \pi R_{\mathrm{L,pinch}}^2 / \lambda = 6.7\,\mathrm{cm}$. In generating this figure a frequency detuning of $\Delta\omega/\omega = -1.5\%$ was used.

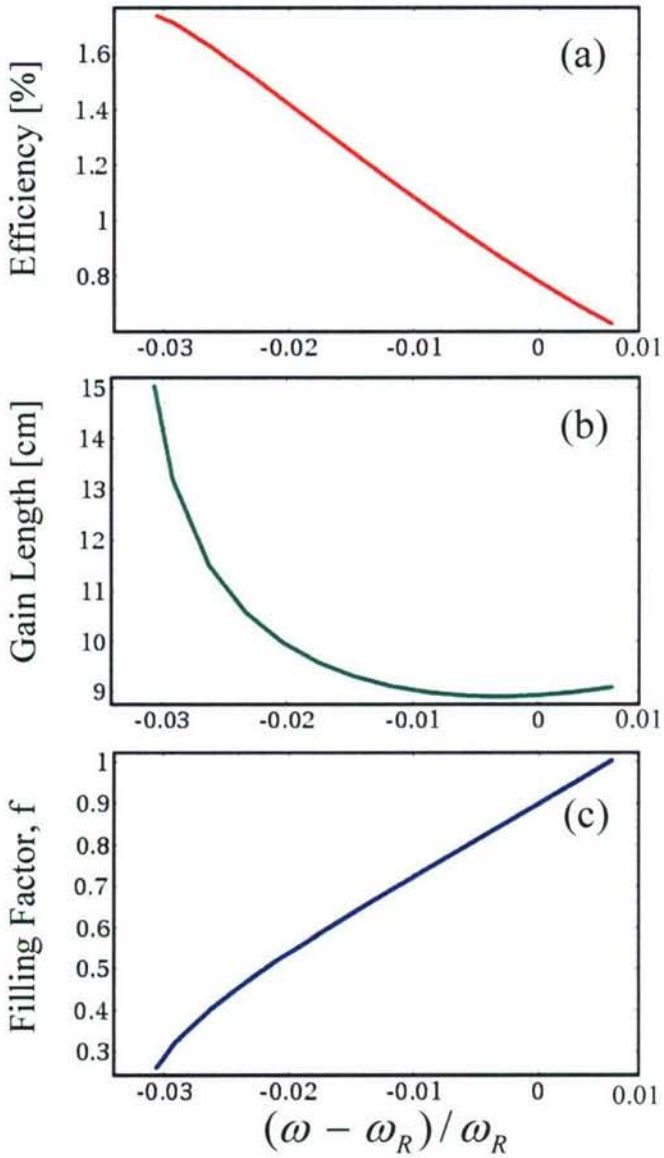


Figure 6: Plots of (a) efficiency, (b) power gain length and (c) filling factor as a function of frequency detuning. The operating frequency is denoted by $\omega$.

**Table I. Wiggler Parameters**

| | | |
|---|---|---|
| Resonant Wavelength, $\lambda$ | 1 μm | 2.141 μm |
| Wiggler Field, $B_W$ | 8.6 kG | 5 kG |
| Wiggler Parameter, $K$ | 1.6 | 1.86 |
| Period, $\lambda_w$ | 2 cm | 4 cm |
| Length, $L_w$ | 1 m | 1.5 m |

**Table II. Electron Beam Parameters**

| | | |
|---|---|---|
| Resonant Wavelength, $\lambda$ | 1 μm | 2.141 μm |
| Energy, $E_b$ | 76 MeV | 81 MeV |
| Current, $I_b$ | 2 kA | 1 kA |
| Radius, $R_b$ | 0.025 cm | 0.02 cm |
| Normalized Emittance, $\varepsilon_{n,rms}$ | 15 mm-mrad | 15 mm-mrad |
| Duty Factor, $D$ | $10^{-3}$ | $1.5 \times 10^{-3}$ |
| RF Linac Frequency | 750 MHz | 750 MHz |
| Micro Pulse Duration | 1.3 psec | 2 psec |
| Betatron Wavelength, $\lambda_B = 2\gamma\lambda_w / K$ | 3.7 m | 7 m |

**Table III. FEL Optical Beam Parameters**

| | | | |
|---|---|---|---|
| Operating Wavelength, $\lambda$ | 1 μm | 2.141 μm | 2.141 μm |
| Frequency Detuning, $\Delta\omega/\omega$ | 0 | 0 | −1.5% |
| Spot Size in Wiggler, $R_L$ | 0.26 mm | 0.33 mm | 0.4 mm |
| Filling Factor, f | 0.9 | 0.36 | 0.25 |
| Rayleigh Range (unpinched, at wiggler exit), $Z_R$ | 22 cm | 16 cm | 23 cm |
| Gain Length (power), $L_e$ | 9 cm | 14 cm | 14 cm |
| Efficiency (uniform wiggler), $\eta$ | 0.8% | 0.77% | 1.2 % |
| Avg. Intensity (unpinched, at wiggler exit), $\langle I \rangle$ | 1.1 GW/cm$^2$ | 0.53 GW/cm$^2$ | 0.58 GW/cm$^2$ |
| Pinched Laser Spot Size, $R_{\mathrm{L,\,pinch}}$ | 0.11 mm | 0.17 mm | 0.21 mm |
| Rayleigh Range (pinched, at wiggler exit), $Z_{\mathrm{R,\,pinch}}$ | 3.6 cm | 4 cm | 6.7 cm |
| Average Pinched Intensity, $\langle I_{\mathrm{pinch}} \rangle$ | 6.7 GW/cm$^2$ | 2.2 GW/cm$^2$ | 2.1 GW/cm$^2$ |
| Peak Output Power, $P$ | 1.2 GW | 0.63 GW | 1 GW |
| Average Output Power, $\langle P \rangle$ | 1.2 MW | 1 MW | 1.5 MW |
| Number of Power e - Folds, $L_w / L_e$ | 11 | 10.6 | 10.5 |
| Average Input Power, $\langle P_{\mathrm{input}} \rangle$ | 18 W | 43 W | 40 W |
| Optical Beam Quality, $M^2$ | 1.5 | 1.5 | 1.5 |

**Table IV. First Relay Mirror Parameters** (for $\lambda$ = 2.141 μm , $\Delta\omega / \omega$ = -1.5%)

| Tilt Angle, Θ [degrees] | 45° | 5° |
|---|---|---|
| Distance from Wiggler (unpinched), $L_{relay}$ [m] | 14 | 5 |
| Distance from Wiggler (pinched), $L_{relay}$ [m] | 8 | 3 |

The average intensity damage threshold was taken to be
$\langle I_{damage} \rangle = 50\,\mathrm{kW/cm^2}$

**Table V. First Relay Mirror Parameters** (for $\lambda$ = 1 μm , $\Delta\omega / \omega$ = 0)

| Tilt Angle, Θ [degrees] | 45° | 5° |
|---|---|---|
| Distance from Wiggler (unpinched), $L_{relay}$ [m] | 27 | 10 |
| Distance from Wiggler (pinched), $L_{relay}$ [m] | 11 | 4 |

The average intensity damage threshold was taken to be
$\langle I_{damage} \rangle = 50\,\mathrm{kW/cm^2}$